Journal of Wind Engineering & Industrial Aerodynamics 175 (2018) 292–304

Contents lists available at ScienceDirect

Journal of Wind Engineering & Industrial Aerodynamics

journal homepage: www.elsevier.com/locate/jweia

Performance assessment of a special Double Skin Façade system for wind energy harvesting and a case study

Sina Hassanli [a,*], Kenny C.S. Kwok [b], Ming Zhao [c]

[a] Centre for Infrastructure Engineering, Western Sydney University, Penrith, NSW 2751, Australia
[b] School of Civil Engineering, The University of Sydney, Sydney, NSW 2006, Australia
[c] School of Computing, Engineering and Mathematics, Western Sydney University, Penrith, NSW 2751, Australia

ARTICLE INFO

Keywords:
Wind energy generation
Double skin façade
Wind turbine
CFD
Wind energy assessment

ABSTRACT

The increasing global concern about climate change and energy crisis has necessitated the development of techniques to reach and exploit renewable energy in unexplored regions. As such, decentralized small-scale wind energy harvesting in urban environments has gained momentum in recent years. In this study, a methodology has been developed to assess the performance of a special Double Skin Façade (DSF) system for wind energy generation using CFD simulations and local wind data. As a case study, a story-high corridor-type DSF system equipped with an array of wind turbines was integrated into a high-rise building, and its Annual Energy Production (AEP) within the context of four Australian cities was evaluated. The results showed that the free-stream wind speed can be amplified up to a maximum of 1.8 times inside the corridors of the DSF system. It was concluded that the benefit of the DSF system can be exploited the most in cities with strong bi-directional wind characteristics. Finally, it was shown that wind turbines inside the DSF system can annually generate up to 50% more energy at open terrain and 22%–45% more energy at dense urban and suburban terrains as compared with the same turbines in the free-stream condition.

1. Introduction

Substantial efforts have been made globally to harvest renewable and clean energy in a variety of scales due to obvious advantages of renewable energy generation from the perspective of reduction in carbon emissions and global warming effects. Many governments have set targets for electricity generation from renewable resources. In Australia, renewable energy contributes to approximately 17.3% of total electricity generation in 2016, with 5.3% sourced from wind energy. It is affirmed by the Australian government to generate 33,000 GWh from large-scale and 4000 GWh from small-scale renewable sources by 2020 (Clean Energy Council, 2016). Small-scale Renewable Energy Scheme (SRES) in Australia supports the installation of new small-scale renewable energy generation systems such as micro wind generators, rooftop solar panels and micro-hydro systems (Clean Energy Regulator, 2015).

As a result of increasing interest in distributed micro-grid renewable energy generation in urban environments, wind resource assessment becomes an essential step to identify suitable sites and potential locations for wind energy generation. To increase the accuracy of the wind energy assessment at localized regions in urban environments, great efforts have been made to develop assessment methods that take into account the buildings height, terrain fabric, and mutual effects between buildings. Mertens (2003) proposed a method to consider the development of an Internal Boundary Layer (IBL) from undisturbed upwind rural area to a built environment when evaluating the wind energy on buildings' roof. Heath et al. (2007) considered the urban boundary layer and described a method to calculate the roughness length and displacement height of this profile for an array of cubes as an urban landscape. Walker (2011) presented a review of existing methods for predicting urban wind speed and wind power production and listed the concerns regarding the accuracy of current methods of estimating power output of micro-scale wind turbines in urban environments.

1.1. Aerodynamic devices in urban environment

Since urban environments generally suffer from low wind speed and high turbulence, it is essential to explore the aerodynamic devices available in urban landscape that can enhance the wind flow to a suitable level for energy generation. In general, potential locations for installing wind turbines in and around buildings, particularly high-rise

* Corresponding author.
E-mail address: S.Hassanli@westernsydney.edu.au (S. Hassanli).

https://doi.org/10.1016/j.jweia.2018.02.002
Received 20 November 2017; Received in revised form 24 January 2018; Accepted 5 February 2018
Available online 23 February 2018
0167-6105/

List of abbreviations

H	building Height
θ	wind direction
β	building orientation from North direction
f_a	wind speed amplification factor
u_c	average mean wind speed over vertical cross-sectional area at the middle of corridor
u_z	free-stream reference wind speed at the height of 10 m above the ground
u_{opt}	optimum wind speed
u	wind speed
P_w	wind power density
$\overline{P}_w$	average wind power density
$\overline{E}_w$	annual energy production
ρ	density
f	probability of occurrence of a wind condition
$f^{'}$	probability of occurrence of a wind speed inside corridors
N	number of wind speed observations
k	shape factor of Weibull function
c	scale factor of Weibull function
n	number of wind turbines
t	total number of operating hours of wind turbine
P_c	power curve of wind turbine inside corridor
P_f	power curve of wind turbine at free-stream
z_0	roughness length

buildings, which accommodate aerodynamic devices can be classified into four categories: (a) on roof, (b) between two buildings, (c) inside through-building openings, and (d) integration into building's skin. A wind turbine can also be placed in a suitable position downstream a low-rise building to take advantage of the enhanced flow as a result of wind passing over the building. The enhancement of the wind speed in these locations is affected by a number of factors such as the height of the building, the roof shape and the shadow effect of surrounding buildings. Table 1 lists recent studies that evaluate wind power in potential locations in and around buildings for wind energy harvesting. The table is mainly presented to compare the methods used in different studies and the parameters included or excluded. The reasons of selecting a method or including a parameter are discussed in the following paragraphs.

Regarding the method, conventional techniques for wind resource assessment involve installing anemometers and on-site measurements (Heath et al., 2007). However, these measurement campaigns are usually lengthy and not economically feasible for small-scale projects (Heo et al., 2016; Yang et al., 2016). Moreover, due to the geometrical complexity of urban environments, wind flow can change substantially over a relatively small distances and thus, the traditional techniques are not capable of mapping the wind flow in an area with a high-resolution (Tabrizi et al., 2014). Computational Fluid Dynamics (CFD) has been proven to be an affordable, effective and more robust alternative for investigating flow characteristics in built environments (Chaudhry et al., 2015; Yang et al., 2016). The growing applications of CFD as a result of growing computational power-to-cost ratio can be recognized in Table 1.

The accuracy of the wind flow simulation and the power of the computing resources are the main factors to be considered when choosing an appropriate CFD method (Ledo et al., 2011; Tabrizi et al., 2014). Hence, there is always a compromise between accuracy and computational cost (Toja-Silva et al., 2015a). Although Large Eddy Simulations (LES) provide more accurate results and better agreement with experimental data, its computational cost is still high, because it needs very high-resolution computational grids. The Reynolds-Averaged Navier Stokes (RANS) equations coupled with a range of suitable turbulent models are commonly used due to their efficiency (Toja-Silva et al., 2015b). Regarding the most accurate RANS turbulence model for simulating the flow in urban environment, mixed conclusions are found (Larin et al., 2016). Nevertheless, the standard and realizable $k-\varepsilon$ models are widely used for modelling atmospheric boundary layer and flow around buildings (Dannecker and Grant, 2002). The Shear Stress Transport (*SST*) $k-\omega$ model has been shown to be able to predict flow separation under adverse pressure gradient more accurate than $k-\varepsilon$ models, and it is more reliable in the case of bounded flow and ducted flow (Ledo et al., 2011; Tabrizi et al., 2014; Watson et al., 2007).

In general, the potential of high-rise buildings for wind energy generation is great because of the high wind velocity around high-rise buildings that have little shadowing effect from the low to mid-rise neighboring buildings (Li et al., 2016a; Park et al., 2016; Toja-Silva et al., 2015a). Low-rise buildings are the main interest in rural areas (White and Wakes, 2014) or in areas with a great number of low to mid-rise buildings (Heath et al., 2007).

'Specific' in Table 1 refers to the target building models that are replicated from real buildings in specific locations. 'Generic' refers to the generic forms of a building which are not necessarily representative of a real building. It is very often the case that surrounding buildings are included in CFD simulations or wind tunnel tests when investigating the flow in or around specific buildings (Balduzzi et al., 2012; Ledo et al., 2011). However, surrounding buildings are often not modelled when the primary focus of a study is the identification of potential locations of installing a wind turbine or the effect of building geometrical characteristics such as roof shape on wind energy harvesting (Balduzzi et al., 2012; Ledo et al., 2011; Yang et al., 2016). Moreover, surrounding low-rise buildings are usually not considered when the target location is a rooftop of a high-rise building (Abohela et al., 2013).

To enhance wind power generation, a wind turbine is often enclosed in a specially designed shroud, known as Diffusor Augmented Wind Turbines (DAWTs). In some especial cases, DAWTs utilize ducted flow and pressure difference in building openings for wind power generation (Hassanli et al., 2018; Toja-Silva et al., 2015a; Watson et al., 2007). The simplification of not modelling the wind turbine is frequently made especially in the case of examining wind energy available on rooftop of buildings and investigating the effect of roof shapes or complex terrain (White and Wakes, 2014).

As indicated in Table 1, when dealing with a generic form of a building, Atmospheric Boundary Layer (ABL) velocity profiles were preferred as the inlet boundary condition for CFD simulation. On the other hand, to model a specific building, Integral Boundary Layer (IBL) profiles that consider a displacement height corresponding to the mean height of surrounding buildings were often used (Heath et al., 2007; Balduzzi et al., 2012).

Apart from having higher velocities, another advantage of rooftop installation is that wind turbines do not occupy the useful space of occupants and can be retrofitted into existing buildings (Chong et al., 2016; Grant et al., 2008). However, turbines should be installed above a minimum height because the separation of flow from building edges generates strong turbulence close to the roofs. Raising turbines to the level where the effect of wind turbulence is weak requires a strong foundation, especially in the case of high-rise buildings, which sometimes is not viable (Kono et al., 2016). Furthermore, there is no control over the directionality of wind, which can also be negatively influenced by the edges of buildings and create large regions of high turbulence and low velocities (Toja-Silva et al., 2013).

Table 1
Non-Exhaustive overview of literature available for wind energy assessment in and around buildings

References	Target Building Model	N. of buildings	Building Type	Modelling of Surrounding Buildings	Turbine Modelling	Enhancement Device modelling	METHOD	CFD Simulation	Turbulence Model	Wind Profile
Rooftop										
(Abohela et al., 2013)	Generic	Single	Low to Mid Rise	Y	N	N	CFD	RANS/3D/SS	RKE	ABL
(Lu and Ip, 2009)	Generic	Multiple	High Rise	N	N	N	CFD/LWD	RANS/3D/SS	SKE	ABL
(Toja-Silva et al., 2015a)	Generic	Single	Mid Rise	N	N	N	CFD	RANS/3D/SS	different RANS	ABL
(Wang et al., 2015)	Generic	Two buildings	Low Rise	N	N	N	CFD	RANS/3D/SS	SKE	ABL
(Mertens, 2003)	Generic	Single	Mid Rise	N	N	N	CFD	RANS/3D/SS	SKE	IBL
(Balduzzi et al., 2012)	Generic	Multiple	Mixed	Y	N	N	CFD	RANS/2D/SS	SKE	IBL
(Watson et al., 2007)	Generic	Single	Low Rise	N	Y	Y	CFD	RANS/3D/SS	SST	ABL
(Tabrizi et al., 2014)	Specific	Single	Low Rise	Y	N	N	CFD/FM/LWD	RANS/3D/SS	SST	
(Heath et al., 2007)	Specific	Multiple	Low Rise	Y	N	N	CFD	RANS/3D/U	SKE	IBL
(Toja-Silva et al., 2015b)	Generic	Single	High Rise	N	N	N	CFD	RANS/3D/SS	SKE	
(Lu and Sun, 2014)	Specific	Single	High Rise	N	N	N	CFD/LWD	RANS/3D/SS	RNG	
(Ledo et al., 2011)	Specific	Multiple	Low Rise	Y	N	N	CFD	RANS/3D/QS	SST	IBL
(Chong et al., 2016)	Generic	Single	Low Rise	N	N	Y	CFD	RANS/2D/SS	–	IB
(Romanic et al., 2017)	Specific	Multiple	Mixed	Y	N	N	CFD/LWD	RANS/3D/SS	SST	IBL
(Yang et al., 2016)	Specific	Multiple	Mixed	Y	N	N	CFD/FM/LWD	RANS/3D/SS	RKE	
(Kim et al., 2016)	Specific	Single	High Rise	Y	N	N	CFD/FM/LWD	RANS/3D/SS	modified k–ε	
(Kono et al., 2016)	Generic	Single	High Rise	N	N	N	CFD	LES	–	
(Larin et al., 2016)	Generic	Single	Low Rise	N	Y	N	CFD	RANS/3D/U	RKE	ABL
(Krishnan and Paraschivoiu, 2016)	Generic	Single	Low Rise	N	Y	Y	CFD	RANS/3D/U	RKE	ABL
(Park et al., 2016)	Specific		High Rise	Y	Y	Y	WT/FS	–	–	
In Between two buildings										
(Lu and Ip, 2009)	Generic	Multiple	High Rise	N	N	N	CFD	RANS/3D/SS	SKE	ABL
(Khayrullina et al., 2013)	Generic	Two Buildings	High Rise	N	N	N	CFD/LWD		RKE	ABL
(Smith and Killa, 2007)	Specific	Two Buildings	High-Rise	N	N	N	Report	–	–	
(Chaudhry et al., 2015)	Generic	Two Buildings	High Rise	N	N	N	CFD/LWD		SKE	ABL
(Heo et al., 2016)	Generic	Two Buildings	High Rise	N	Y	N	CFD	URANS	SST	ABL
Through-building openings										
(Li et al., 2016b)	Specific	Single	High Rise	Y	N	Y	WT/LWD	–	–	ABL
(Hassanli et al., 2016)	Generic	Single	High Rise	N	N	Y	CFD	RANS/3D/SS	SST	ABL
(Dannecker and Grant, 2002)	Generic	Single	–	N	N	Y	CFD/WT/LWD	RANS/3D/SS	SKE	
Integration into building's skin										
(Park et al., 2015)	Generic	Single	High Rise	N	Y	Y	CFD/WT/LWD	RANS/2D/SS	SKO	Uniform
(Hassanli et al., 2017a)	Generic	Single	High Rise	N	N	Y	CFD/WT	RANS/3D/SS	SST	ABL
Adjacent to building										
(Padmanabhan, 2013)	–	–	–	N	N	Y	CFD/FS	RANS/3D/SS	SKE	Uniform
(White and Wakes, 2014)	Generic	Single	Low-Rise	N	N	N	CFD	RANS/3D/SS	SKE	ABL

RANS = Reynolds-Averaged Navier Stokes, URANS = Unsteady RANS, LES = Large Eddy Simulation. LWD = local wind data, FM = field measurement, FS = full scale, WT = wind tunnel, 3D = three dimensional, 2D = two dimensional, SS = Steady-State, QS = Quasi-State, U=Unsteady, SKE = Standard k–ε model, RKE = Realizable k–ε model, RNG = RNG k–ε model, SKO = Standard k-ω, SST = SST k-ω model, ABL = Atmospheric Boundary Layer profile, IBL = Internal Boundary Layer Profile.

1.2. Special Double Skin Façade for wind energy harvesting

Hassanli et al. (2017a) proposed an alternative approach by utilizing the cavity flow of a special Double Skin Façade (DSF) system with strategic openings for harvesting wind energy in urban environment. A different application of the same DSF concept for wind-induced response reduction of high-rise buildings was proposed by Hu et al. (2017). A DSF is a façade consisting of two distinct planar elements separated by an air cavity, which is conventionally used for thermal and sound insulation, ventilation, and aesthetics. They conducted a series of wind tunnel tests and CFD simulations to investigate the flow characteristics and the associated flow mechanisms inside the cavity of DSF for different wind directions. The results showed that flow inside the cavity is unidirectional and relatively uniform, which is a suitable condition for generating power specially in the case of Horizontal Axis Wind Turbines (HAWTs). It was also concluded that the DSF system can effectively enhance the flow within the cavity for a wide range of wind directions. Following the previous studies, Hassanli et al. (2018) studied the effect of four aerodynamic modifications including recessed regions and curved walls on the flow characteristics inside a corridor-type DSF. It was found that the flow turbulence inside the corridors could be reduced by about 30% by the modifications. More importantly, the average available power density of a corridor-type DSF could be increased by a factor of 2 and 4.2 by creating recessed regions and curved walls, respectively. While the efficiency of the modified DSF system was demonstrated, the energy yield of the system in a real condition by integrating local wind data needed to be evaluated. Furthermore, the criteria and the method of wind turbine selection had to be addressed, and the effect of confined area on the performance of the wind turbine had to be assessed.

This study presents a methodology to assess the wind energy yield inside a special DSF system integrated with a high-rise building. As a case study, the local wind data of four major cities in Australia including Sydney, Melbourne, Brisbane and Adelaide were incorporated with CFD simulations to evaluate the Annual Energy Production (AEP) of the DSF system. First, the amplification of wind velocity inside the corridors of the DSF system at different reference wind speeds and different wind directions is studied, and the wind power using the equal probability of wind coming in any directions is calculated. Second, the estimated wind power inside corridors of the DSF system at different building orientations in the four cities is investigated. Third, the probability distribution of wind velocity inside the corridors at the best building orientation in each city is determined. Fourth, an appropriate wind turbine is selected with rated speed close to the optimum velocity inside the corridors. Fifth, for each city, the AEP of a set of selected wind turbines inside the DSF system is compared with the AEP of the same wind turbines in a free-stream condition. Finally, the impact of the terrain roughness in each city on the AEP of the building is evaluated.

It is important to note that in windy days, the wind force is likely to be dominant compared with the buoyancy force even for conventional DSFs with top and bottom openings (Barbosa and Ip, 2014). If the DSF is properly designed to take advantage of wind pressures at the inlet and outlet, wind pressure dominates airflow rate (Poirazis, 2004). This is the case for our proposed DSF that utilizes strategic openings based on pressure difference. Therefore, thermal effects are expected to have a negligible effect on airflow rate, and consequently, it is not considered. Also, it is worth noting that high airflow rate due to wind pressure difference means a higher ventilation rate within the cavity. This would increase the convective heat transfer between flow and the interior skin. Depending on the conditions of outside and inside, this may result in increase or decrease in temperature inside the building. However, this is not within the scope of this paper.

2. Methodology

Hassanli et al. (2017a) conducted a series of experimental and numerical investigations of the flow characteristics and the mechanism of flow entering and discharging the cavity of a DSF with strategic openings at different wind directions. Recently, Hassanli et al. (2018) studied the enhancement of wind energy harvesting via aerodynamic modifications of a corridor-type DSF system and compared the performances of three aerodynamic modification layouts. In this study, the layout with the best performance identified by Hassanli et al. (2018) was selected for the study reported in this paper.

2.1. Description of building model and DSF system

A 1:150 scale model of a Commonwealth Advisory Aeronautical Council (CAARC) standard tall building model was considered (Fig. 1*a*). The size of the model building was 1 200 *mm* × 300 *mm* × 200 *mm* (prototype: 180 *m* × 45 *m* × 30 *m*). DSFs at the two opposite longer sides of the building model with a 13.3 *mm* gap (prototype: 2 *m*) were employed. Dividing the cavity of the DSF by two horizontal walls created 26.6 *mm* high corridors at the selected height of 1000 *mm* as shown in Fig. 1. The corridors are one-story high (prototype: 4 *m*). An opening was created in the central part of the external façade. The sides of the DSF are open to exterior environment. By creating openings, four corridors labelled as C1, C2, C3 and C4 were formed (Fig. 1*b*). The wall sections in between two horizontal divisions of each corridor at two opposite smaller sides of the building were recessed 13.3 *mm* (prototype: 2 *m*) and the corridors' inner corners were rounded with the radius of 26.7 *mm* (prototype: 4 *m*) (Fig. 1c). Four modifications as compared with the original building-high single-sided DSF considered in the study by Hassanli et al. (2017a) were employed: 1- double-sided DSF, 2- corridor-type DSF, 3- recessed regions, and 4- curved walls. In the study by Hassanli et al. (2018), it was shown that the elevation of the corridor has a little effect on the velocity inside the corridor, as long as the corridor is located at the top third of the building height and is not very close to the roof. Therefore, the corridors were created at 0.83*H* in this study, where *H* refers to the building height. While all 15 floors at the top third of the CAARC building model or a strategic selection of floors could be employed for wind energy harvesting, the energy yield of a one story-high DSF is assessed here.

The flowchart of the steps taken for the wind energy assessment of the DSF system is depicted in Fig. 2. The steps including computational domain, boundary conditions, turbulence model, mesh independence study, and CFD validation were discussed in the previous study (Hassanli et al., 2018). Based on these steps, the steady-state SST k-ω turbulence model to predict the mean flow characteristics inside the cavity of DSF has been considered. The computational domain extensions and boundary conditions are shown in Fig. 3. Based on the detailed grid independence analysis in the same study, the domain is constructed with about 7 million fully-structured hexahedral elements.

2.2. Method of incorporating local wind data

In addition to the previous steps, the following steps were taken specifically for the present study:

Step 1: Investigate flow characteristics inside DSF at different wind directions

A series of CFD simulations were performed by considering a range of reference wind speeds between 3 *m/s* and 30 *m/s* at 10 *m* height and wind directions between 0° and 180° with a 22.5° interval. The wind speed amplification factor (f_a) was defined as the ratio of the average mean wind speed over the cross-sectional area at the middle of each corridor, u_c to the incoming reference wind speed at the height of 10 *m* above the ground, u_z:

$$f_a = u_c/u_z \tag{4}$$

To demonstrate the directional characteristic of the DSF, the total wind power was evaluated by considering the equal probability of wind

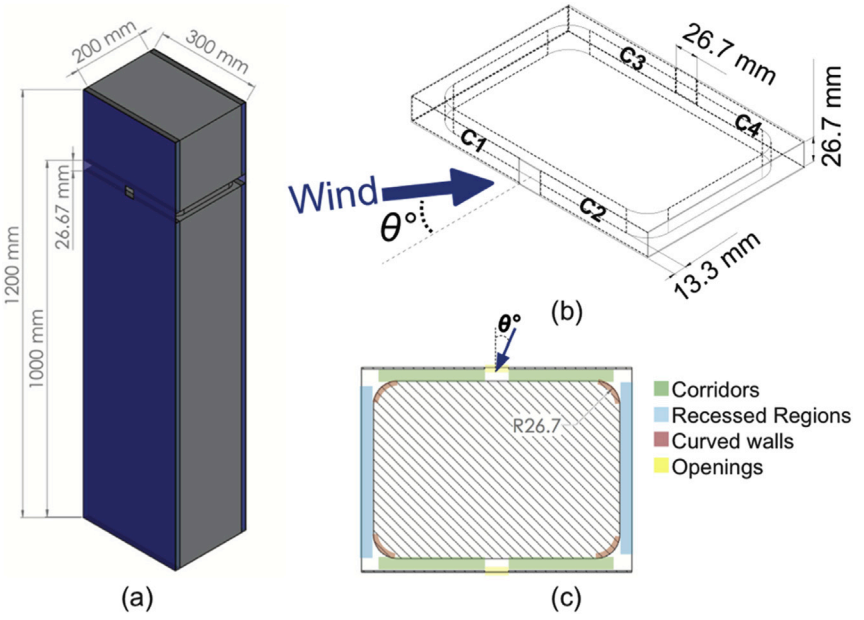

Fig. 1. The model geometry and dimensions, (a) building model (b) isolated DSF system and locations of corridors of DSF against incoming wind, and (c) plan view of DSF

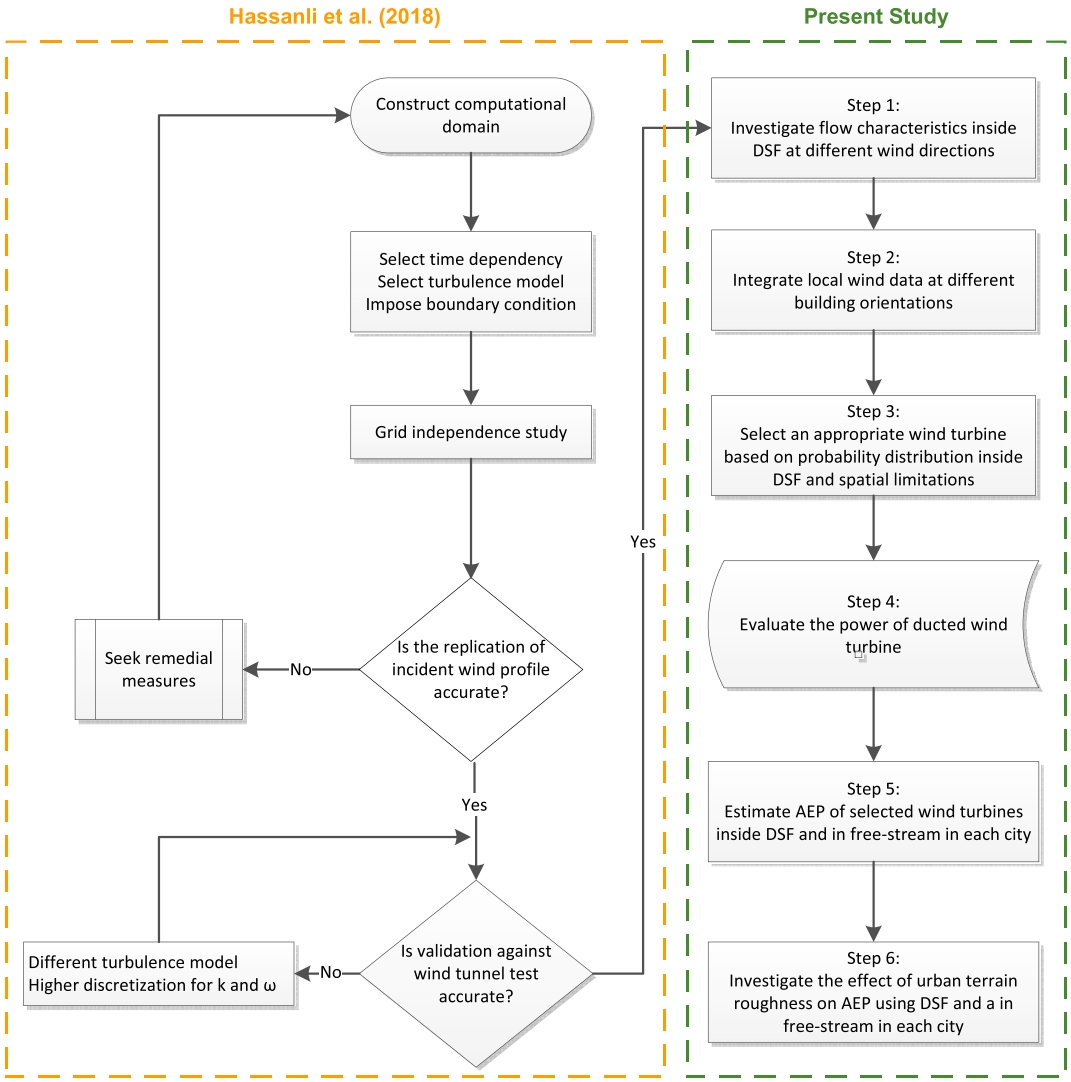

Fig. 2. Flowchart of CFD methodology: Hassanli et al. (2018) and present study

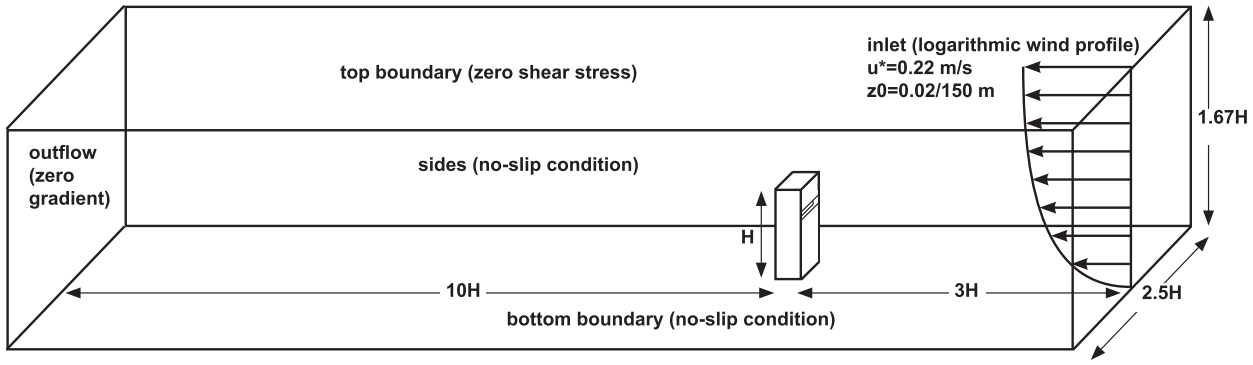

Fig. 3. Computational domain extensions and boundary conditions (Hassanli et al., 2018)

coming in any direction.

Step 2: Integrate local wind data at different building orientations

Wind power density, measured in *Watt per square meter*, as an important indicator of available wind energy at a potential location, can be expressed as:

$$P_w = \frac{1}{2}\rho u^3 \tag{5}$$

where ρ is the density of the air and u is the wind speed. Considering a constant air density, the average wind power density can be evaluated by integrating the product of the wind power density and the probability density of wind over all possible speeds and directions:

$$\overline{P}_w = \int_{0^\circ}^{360^\circ}\int_0^{u_{max}} \frac{1}{2}\rho u^3 f(u,\theta)\, du\, d\theta \tag{6}$$

The probability density function, $,f(u,\theta)$, is the probability of occurrence of a wind condition defined by wind speed, u and wind direction, θ. It can be determined by fitting the function to the local mean wind data. In the case of two variants, u and θ, one of the parametric bivariate density functions including isotropic or anisotropic Gaussian models (Carta et al., 2008) or a non-parametric density function such as Kernel density estimation (Zhang et al., 2013) can be used to determine $f(u,\theta)$. In this study, the averaged power is determined using the direct method of wind data analysis. Therefore, the wind data is presented as a set of N discrete wind speed observations and a set of M wind direction observations, the average wind power density inside the corridors can be determined as:

$$\overline{P}_w = \sum_{i=1}^{N}\sum_{j=1}^{M} \frac{1}{2}\rho u_i^3 p(u_i,\theta_j) \tag{7}$$

where $p(u_i,\theta_j)$ is the frequency of a wind condition defined by wind speed, u_i and wind direction, θ_j at a particular site or location. u_i is the wind speed inside the corridors obtained by conducting a number of CFD simulations explained in step 1. Multiplying the average wind power density defined in equation (7) by the areas of interest results in the average wind power. The area of interest is the cross-sectional area at the middle of each corridor in the one story-high DSF system. The average wind power is then calculated for different orientations of the building model to find the best building orientation in a particular wind climate.

Step 3: Select an appropriate wind turbine based on probability distribution inside DSF and spatial limitations.

Using bins method and accumulating the probabilities of wind speeds with equal magnitude, the probability distribution of wind speeds inside the corridors can be found based on a local climate data. Because the wind in the corridors is unidirectional, the average wind power density can be simplified to:

$$\overline{P}_w = \int_0^{u_{max}} \frac{1}{2}\rho u^3 f'(u)\, du \tag{8}$$

where $f'(u)$ is the probability of a wind speed, u, inside the corridors. $f'(u)$ can be estimated with the Weibull function which is a two-parameter probability density function and can be used to describe the wind speed frequency curve:

$$f'(u) = \left(\frac{k}{c}\right)\left(\frac{u}{c}\right)^{k-1} \exp\left[-\left(\frac{u}{c}\right)^k\right] \tag{9}$$

where k and c are the shape and scale factors and both can be determined by fitting the curve into the data. Note that $1/2\rho u^3 f'(u)$, in equation (8), has a peak at some wind speeds called optimum velocity, u_{opt}. Optimum velocity is the velocity that produces more energy than any other wind speed and can be determined by setting the derivative of $u^3 f'(u)$ to zero and solve u. By using the Weibull function, the optimum velocity can be simplified to:

$$u_{opt} = c\left(\frac{k+2}{k}\right)^{\frac{1}{k}} \tag{10}$$

The optimum wind speed u_{opt} is an appropriate parameter for wind turbine selection. A wind turbine should be selected that has the rated wind speed close to the optimum wind speed and also meet the geometrical considerations of the confined area of the corridor.

Step 4: Evaluate the power of ducted wind turbine

To assess the actual wind power of the selected wind turbine, we cannot rely on the turbine manufacturer's power curve as these measurements are collected in a free-stream condition rather than in a confined area (Hassanli et al., 2017b; Jafari et al., 2017). Hence, a few CFD simulations were performed by explicitly modelling the wind turbine at free-steam to validate the CFD results and inside a corridor to acquire the power curve of the wind turbine in a corridor as a representative of a confined area. The tip speed ratio of the blades at each wind speed was set according to the practical RPM curve in free-stream. The resultant torque exerted on the blades was then calculated and multiplied by the rotating speed resulting in the power generation.

Step 5: Estimate AEP of selected wind turbines inside DSF and in free-stream in each city

Not all the wind power available will be converted to the energy due to the limitations associated with the wind turbine. Below a certain wind speed known as cut-in speed, there is an insufficient torque applied by the flow on blades to rotate and therefore, the wind turbine does not

generate electricity. Beyond the cut-in speed, the power increases by increasing the wind speed until it reaches the maximum power at the rated speed. Beyond that, the power decreases slightly with increasing the wind speed until the cut-out speed where a brake system either stops the blades from rotating or reduces the rotating speed to avoid damage to the blades. The AEP of an array of the wind turbines at each corridor at the best building orientation in a specific local climate can be calculated as:

$$\overline{E}_w = n \times t \int_0^\infty P_c(u)\, f^{'}(u) du \tag{11}$$

where n is the number of wind turbines that can be fitted as an array at the cross-sectional area of the corridors, t is the total number of hours that the wind turbine is operating, and $P_c(u)$ is the power curve of the wind turbine inside corridors. The AEP of wind turbines inside corridors can then be compared with the AEP of wind turbines at free-stream that can be estimated as:

$$\overline{E}_w = n \times t \int_0^\infty P_f(u)\, f(u) du \tag{12}$$

where $P_f(u)$ is the power curve at free-stream provided by the manufacturer and $f(u)$ is probability density of wind speeds at the local climate.

Step 6: Investigate the effect of urban terrain roughness on the AEP of wind turbines inside DSF and in free-stream in each city

The impact of terrain roughness can be assessed by considering Terrain Category (TC) 2, 3 and 4, specified in Australian Standards AS/NZS 1 170.2:2011. The description of each terrain category with its roughness length, z_0, is depicted in Table 2. The AEP can then be compared with free-stream wind energy generation at the same height and in the same terrain category.

2.3. Apply the method on the cases under study

Four Australian cities: Sydney, Melbourne, Brisbane and Adelaide were selected as case studies. The probability distributions of hourly mean wind speeds with direction for each city at 45° intervals are given in Fig. 4 city, which highlight the different directional characteristics of prevailing wind in each city.

More detailed analysis of probability distributions with an interval of 22.5° (courtesy of MEL Consultants) has been incorporated with the CFD simulations results to determine the average power available at each corridor and total power at different building orientations in 22.5° intervals. By comparing the total power available at different building orientations, the best orientation was determined for each city. Based on the best building orientation in each city, the probability distributions of mean wind speeds inside the corridors for the four studied cities were determined. The shape factor, k, and the scale factor, c, of the Weibull function for each city were determined by fitting the function to the probability distribution of mean wind speeds inside each corridor.

Table 2
Terrain categories and roughness lengths in AS/NZS 1 170.2

Terrain Category	Roughness Length, z_0 (m)
TC1. Exposed open terrain with few or no obstructions and water surfaces at serviceability wind speeds	0.002
TC2. Water surfaces, open terrain, grassland with few, well scattered obstructions having heights generally from 1.5 to 10 m	0.02
TC3. Terrain with numerous closely spaced obstructions 3–5 m high such as areas of suburban housing	0.2
TC4. Terrain with numerous large, high (10–30 m high) and closely spaced obstructions such as large city centres and well-developed industrial complexes	2

Subsequently, the optimum wind speed was calculated using k and c for each corridor and each city.

Based on the optimum wind speed and the cross-sectional area of the corridor, a specific Horizontal Axis Wind Turbine (HAWT), Ampair 300, was selected with the rated wind speed within the range of optimum wind speeds calculated for different corridors and different cities. Fig. 5 shows the power generation of Ampair 300 against the wind velocity provided by the manufacturer and computed by the CFD in free-stream and inside a duct. The turbine was placed inside a duct with the same cross-sectional area as the corridors of the DSF. The rated power of the ducted turbine increased by about 100% and the rated speed increased moderately from about 12.5 m/s to 14.5 m/s. The underlying reason for such behaviour is that, comparing with the free-stream condition, enhanced wind speed within the confined area increases the thrust on the blades, resulting in a higher torque and consequently higher power generation. By having the power curve of the ducted wind turbine and the frequency of wind speeds inside the corridors, the average wind power can be calculated.

Six wind turbines with the rotor diameter of about 1 m in an array of 2 by 3 at the middle vertical plane of each corridor were considered. The AEP of an array of the wind turbines in each corridor at the best building orientation in each city was calculated and compared with the AEP of the same number of wind turbines at the same height in a free-stream condition. Finally, the impact of surface roughness by considering TC2, TC3 and TC4 was assessed for each city and the AEP was compared with the free-stream wind energy generation at the same height and in the same terrain category.

3. Result and discussion

3.1. Cavity flow characteristics of the DSF

A number of CFD simulations were conducted to investigate wind characteristics inside the corridors of the DSF system located at a representative height of 0.83H. The wind speed amplification factor, f_a, was defined as the ratio of the averaged mean wind speed over the cross-sectional area at the middle of each corridor to the reference wind speed at the height of 10 m above the ground, that is the standard height used for collecting local wind data in Australia. The amplification factor inside the four corridors at different incident wind speeds in steps of 1 m/s and directions with the interval of 22.5° is given in Fig. 6. When wind blows within the range of 45° to the corridor axis ($45^\circ < \theta < 135^\circ$ and $225^\circ < \theta < 315^\circ$), f_a is higher than other wind directions. f_a at this range is about 1.5–1.8 in the leading side. Due to the flow discharging from the central opening within this range, the wind velocity decreases channelling from the leading side to the trailing side corridor. The discharging flow rate at the central opening is also a function of wind direction.

Due to the corridor offset from centre of the building, the wind speeds inside each corridor are not symmetrically distributed at wind directions as seen in Fig. 6. However, the wind speeds inside the corridors have a mirror characteristic and therefore, the graphs of C2 and C4 are the mirror images of C1 and C3 with regards to y axis and the graphs of C3 and C4 are the mirror images of C1 and C2 with regards to x axis.

To find the effects of the reference wind speeds on the amplification factor, a series of CFD simulations at different reference speeds were conducted. It is found that the greater reference wind speed results in a higher amplification factor. In general, the increase in the amplification factor at favourable wind directions ($45^\circ < \theta < 135^\circ$ or $225^\circ < \theta < 315^\circ$) is 10%–20% when the wind speed increases from 3 m/s to 30 m/s. However, from Fig. 6, it is found that the change rate of the amplification factor decreases with increasing wind speed suggesting that the curve tends to reach a plateau and converge to a maximum amplification factor, which is believed to be the maximum potential of the DSF system with the current aerodynamic modifications to amplify the wind speed.

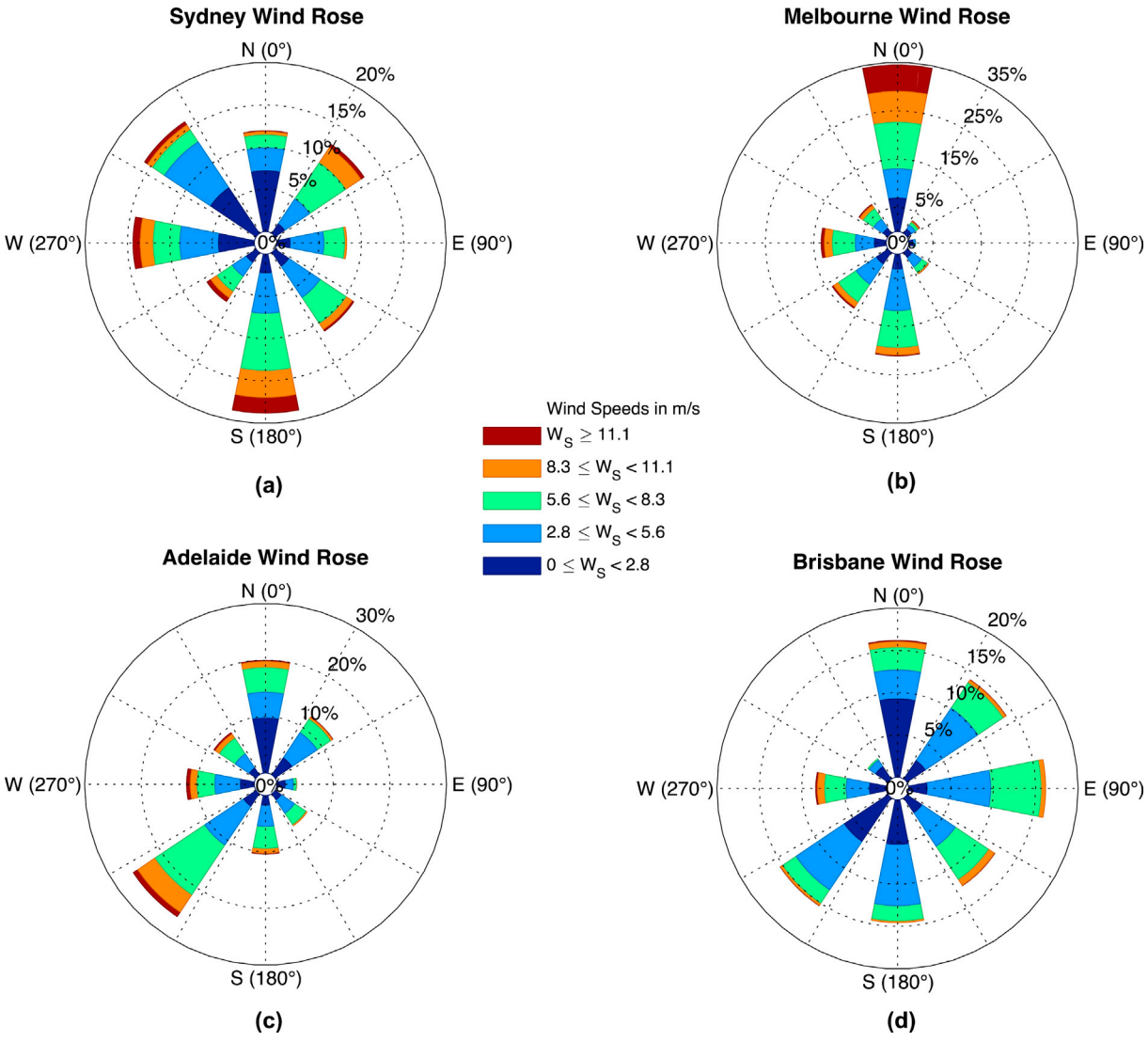

Fig. 4. Wind rose of the four Australian cities: (a) Sydney, (b) Melbourne, (c) Adelaide, and (d) Brisbane (Wind roses for selected locations in Australia, n.d.)

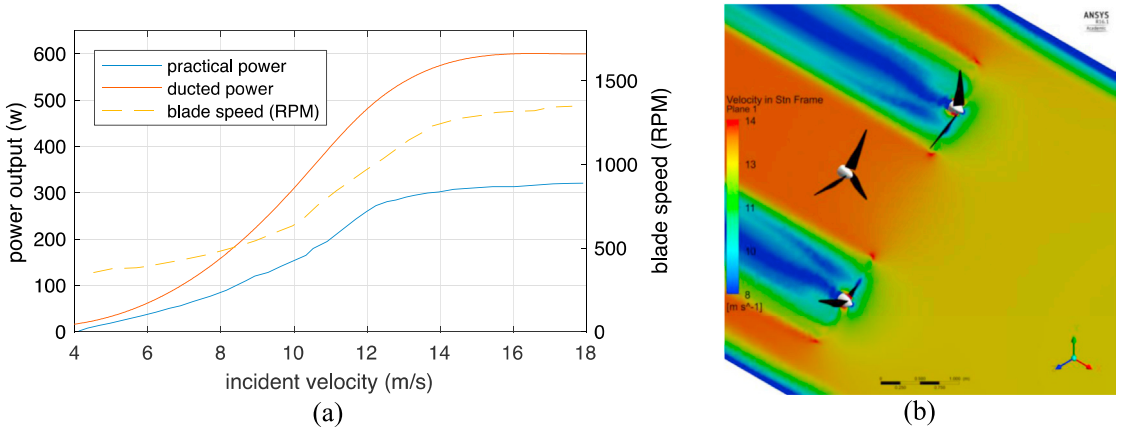

Fig. 5. (a) Power curve and RPM of Ampair 300 in free-stream and inside a duct, and (b) velocity contours around the blades

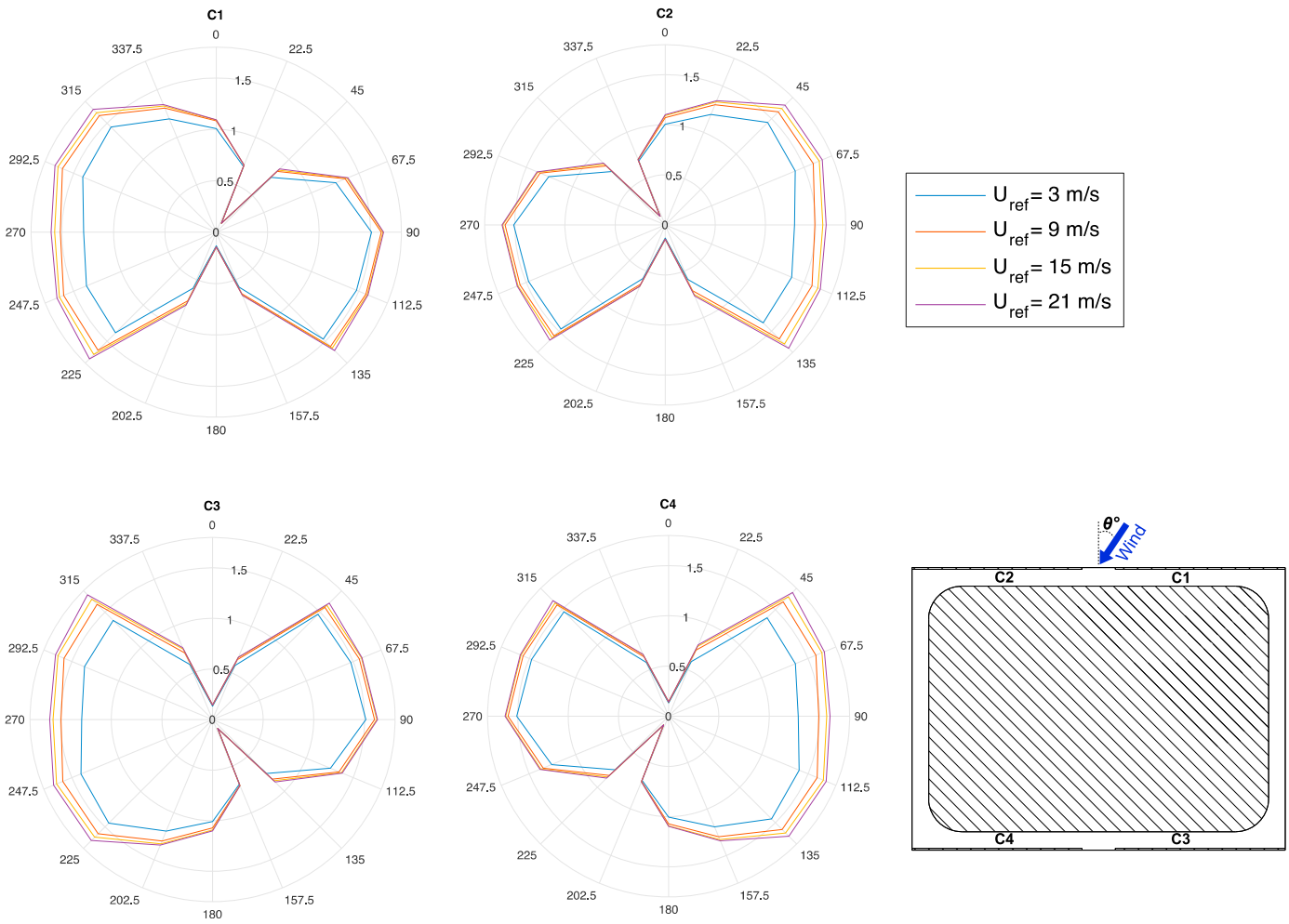

Fig. 6. The wind speed amplification factor, f_a, of the four corridors at different incident wind angle, θ

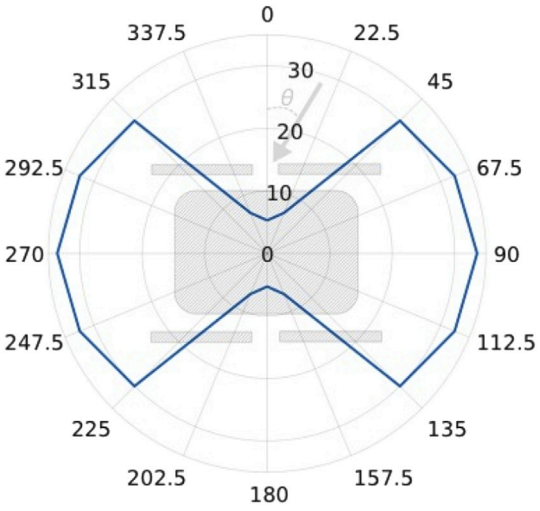

Fig. 7. Total wind power, $\overline{P}_w A$, in KW available at all corridor in different wind directions considering equal probability of wind in all directions

3.2. Wind power characteristics of the DSF

Considering the equal probability of wind coming in any direction, the sum of the available wind power of all corridors at different wind directions is shown in Fig. 7. This is a suitable representation of the directional characteristic of the DSF system that exhibits strong bi-directional enhancement of flow at $45° < \theta < 135°$ and $225° < \theta < 315°$. At $\theta = 0°$, the wind power available is about 5 KW. It increases by a factor of 6 to about 30 kW at 45° and by a factor of 6.6 to about 33 kW at 90°. Within the ranges of 90°±45° and 270°±45° the value of total power changes insignificantly, indicating the relative insensitivity of total power to the wind direction at this range.

3.3. Integration with local wind data

While Fig. 7 provides useful information about the directional characteristic of the DSF system based on the assumption of equal probability of wind coming in any direction, it does not specify the actual average wind power based on the local climate data. Using equation (7), the probability distribution of the hourly mean wind speed in Sydney, Melbourne, Brisbane and Adelaide in Fig. 4 was incorporated to CFD simulations. The building orientation angle, β, is defined as the angle between the corridor axis and the North direction, changing from 0° to 90° with a 22.5° interval. Due to the symmetry of the DSF system with regards to both x and y axes, this range of building orientation was adequate to map the wind power in all directions. The estimated wind power at different building orientations and different corridors are given in Fig. 8a, b, c, and d for Sydney, Melbourne, Adelaide and Brisbane, respectively.

In Sydney (Fig. 8a), the total wind power is about 7.4 $KW \pm 0.4$ KW regardless of the building orientation, indicating the omni-directional characteristic of the DSF system located in Sydney. The insensitivity of the total wind power in the corridors to the building orientation can be an important factor from architectural and construction point of view

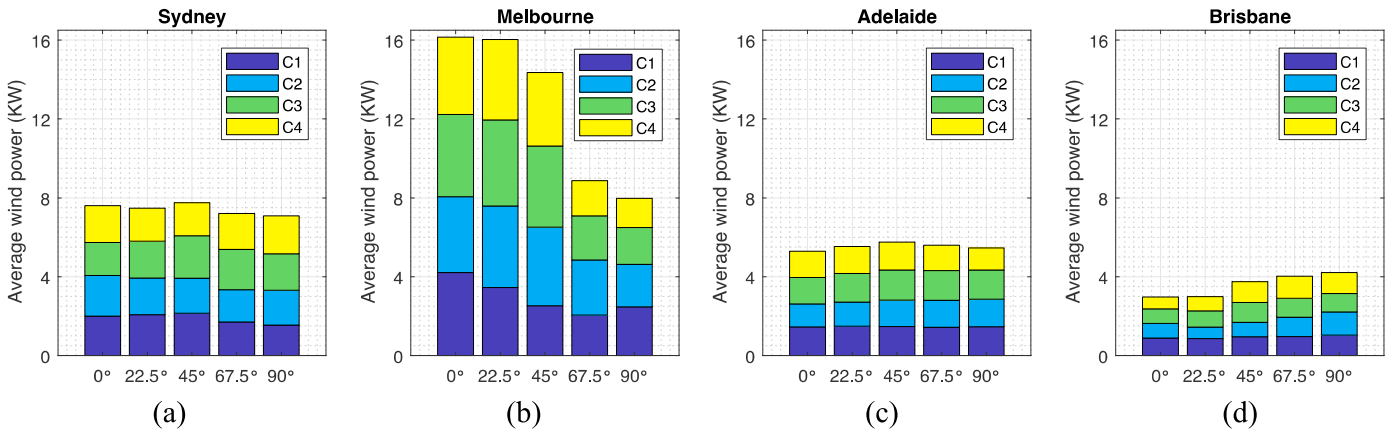

Fig. 8. Wind power at the four corridors at different building orientations in (a) Sydney, (b) Melbourne, (c) Adelaide, and (d) Brisbane

because it does not impose a restriction to the optimal orientation that the building should be constructed. In Melbourne (Fig. 8b), however, the wind power varies significantly with changing β. The wind power at $\beta = 0^\circ$ (the corridor axis is in the North-South direction) is the greatest and it decreases with increasing β until hits its minimum at $\beta = 90^\circ$. In fact, the total wind power decreases from about 16 kW at $\beta = 0^\circ$ to about 8 kW at $\beta = 90^\circ$. This bidirectional characteristic of the DSF system in Melbourne illustrated in Fig. 9 is attributed to the strong North-South wind in this region as shown in Fig. 4b. In Fig. 8c, the total wind power at different wind directions in Adelaide remains about 5.8 $KW\pm$ 0.15 KW, indicating the omni-directionality of the DSF system in this region. In Fig. 8d, the wind power of the DSF system in Brisbane at $\beta = 0^\circ$ is estimated to be about 3 KW and increases to the maximum of 4.2 kW at $\beta = 90^\circ$, showing an East-West bi-directional characteristic of the DSF system in this region.

By comparing the total wind power at different cities in Fig. 9, it can be seen that the DSF system in Melbourne can generate 16 KW wind power at $\beta = 0^\circ$, twice as much as the second greatest wind power generated by DSF system in Sydney. Melbourne is the most suitable Australian city for the application of the novel DSF system. Sydney comes

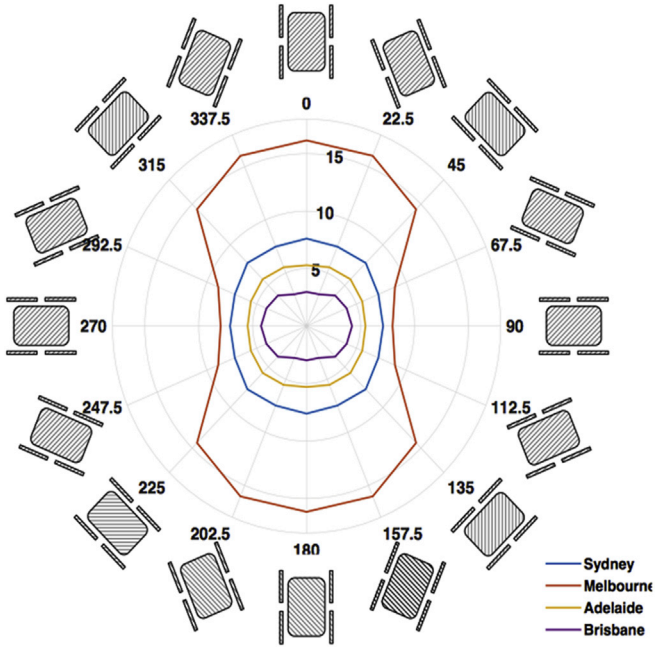

Fig. 9. Total wind power available in KW at all corridors at different building orientations in Sydney, Melbourne, Adelaide and Brisbane

in the second by achieving about 7.8 kW at its best building orientation ($\beta = 45^\circ$). The estimated maximum wind power in Adelaide is 5.8 KW with the same building orientation as Sydney. Brisbane with the maximum total wind power of about 4.2 kW at $\beta = 90^\circ$ is the least preferred city.

Based on Fig. 8, it should also be pointed out that at the best building orientation of each city, the wind power inside the corridors is very close to each other, which means that all corridors contribute almost evenly in generating power. Therefore, the same wind turbine can be implemented in different corridors and the torque on the blades of turbines located at different corridors would be similar.

3.4. Wind turbine selection

The probability distribution of wind speeds inside the corridors of the DSF was calculated for the best building orientation of each city (i.e. $\beta = 45^\circ$,0°, 45°, and 90° for Sydney, Melbourne, Adelaide and Brisbane, respectively). Based on the fitted Weibull density functions, the two coefficients of k and c were calculated for each corridor and each city as given in.

The mean velocity, $\bar{u}$, and the optimum velocity, u_{opt}, inside each corridor were calculated based on k and c presented in Table 3. The mean velocity inside the corridors is within the range of 4.6–6.4 m/s and the optimum velocity is within the range of 10–16.5 m/s. Based on the results, Ampair 300, with the rated wind speed of about 12 m/s was selected for this study.

3.5. AEP based on the HAWT

The AEP representing the energy generation budget of a story-high DSF system equipped with the HAWTs at the best building orientation in each city is given in Fig. 10. While the total power available at all corridor in each city (Fig. 8) was calculated based on equation (7), in this section the ducted power curve of Ampair 300 and the probability distribution of mean wind speeds inside the corridors were considered to evaluate the AEP based on equation (11). The AEP of the DSF system oriented at $\beta = 45^\circ$ located in Sydney is about 20 MWh, with each corridor contributing about 5 ± 0.3 MWh. The energy extracted by the wind turbines is about 28% of the average wind energy available inside all corridors of the DSF system in Sydney shown in Fig. 8a and is almost 30% greater than the AEP that could be generated with the same number wind turbines at the same height in a free-stream condition. The AEP of wind turbines in each corridor of the DSF system located in Melbourne on average is about 8.6 ± 0.4 MWh at $\beta = 0^\circ$. The production in all corridors is very close to each other and all together generate 34 MWh energy, approximately 50% more than that in a free-stream condition. The energy extracted by the wind turbines is approximately 25% of the average

Table 3
Shape factor, scale factor, mean velocity, and optimum velocity inside each corridor of DSF in each city

	Sydney				Melbourne			
	C1	**C2**	**C3**	**C4**	**C1**	**C2**	**C3**	**C4**
c	5.9	5.44	6.47	5.1	7.98	7.06	7.32	6.84
k	1.28	1.34	1.22	1.16	1.49	1.44	1.21	1.25
$\bar{u}$ (m/s)	5	6.06	4.84	7.21	6.41	6.88	6.37	4.13
u_{opt} (m/s)	12.29	10.79	14.35	12.04	14.13	12.94	16.47	14.68
	Adelaide				**Brisbane**			
	C1	**C2**	**C3**	**C4**	**C1**	**C2**	**C3**	**C4**
c	4.37	4.26	4.7	4.05	3.63	4.65	3.97	4.17
k	1.18	1.17	1.27	1.1	1.05	1.22	1.2	1.22
$\bar{u}$ (m/s)	4.03	4.37	3.91	3.56	4.36	3.74	3.91	4.38
u_{opt} (m/s)	10.08	9.97	9.94	10.37	9.99	10.34	9.03	9.26

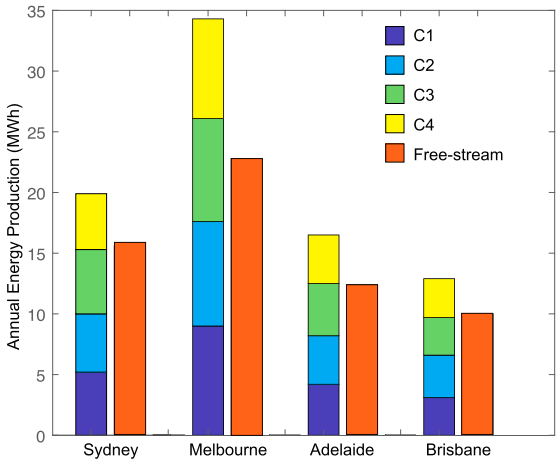

Fig. 10. Annual Energy Production of the HAWTs integrated into the DSF system located in Sydney, Melbourne, Adelaide, and Brisbane

wind energy available inside the corridors in Melbourne shown in Fig. 8b. The AEP in Melbourne is about 70% more than that in Sydney. The AEP of the DSF system oriented at $\beta = 45^{\circ}$ in Adelaide at each corridor on average is about 4.2 ± 0.2 MWh. The AEP in total is approximately 16.5 MWh, 34% greater than the total wind power generated with the same number of the wind turbines at the same height in a free-stream condition. The wind turbines could extract about 32% of the average wind energy available inside the corridors in Adelaide shown in Fig. 8c. The AEP in Brisbane at each corridor is about 3.3 ± 0.2 MWh. The AEP is about 13 MWh, indicating that 35% of the average wind power available at all corridors can be extracted with the wind turbines. The AEP is 28% greater than the AEP generated in a free-stream condition.

In conclusion, in the case of the building model located in open terrains, wind energy harvesting by the DSF in all the studied cities is 30%–50% greater than that in a free-stream condition. It is noteworthy to mention that the installation of this number of wind turbines at free-stream at the height corresponding to the corridor's height requires a very strong supporting system and may not even be economically viable. Moreover, the direct effect of wind turbine on the flow inside the corridors has not been considered in this study.

It is important to also note that the estimated AEP is based on one story-high corridor-type DSF. The advantage of this system is that the wind energy can be exploited at all or selective floors of a building. It was concluded in the previous study (Hassanli et al., 2018) that the average wind speeds inside corridors of different floors within the top-third height of the building, except the few floors close to the roof, was very similar to each other. Therefore, with an appropriate design of DSF for harvesting purposes, almost all 15 floors at the top-third height of the current 45-stroy building model can be utilized for wind energy harvesting. Consequently, in the case of utilizing the DSF system integrated into the CAARC building in Melbourne region, there is a potential to achieve the maximum AEP of 450 MWh.

3.6. AEP at different terrains

The AEP calculated in the previous section was for open terrains specified as TC2 in the Australian Standards *AS/NZS 1 170.2:2011*. It is important, however, to determine the AEP for other terrain categorises especially TC3 and TC4, due to the higher chance of construction of high-rise buildings in suburban area and dense metropolitan regions. Based on the log-law formula, by changing the terrain category from 2 to 3 and 4, the wind speed at the corridors' height reduces 13% and 31% and the wind power available at this height drops 34% and 68%, respectively.

The effect of the terrain category on the AEP of the wind turbines integrated with the DSF system and the AEP in a free-stream condition in the four cities is shown in Fig. 11. As can be seen, the AEP reduces by increasing roughness of the terrains in all four cities. However, the AEP of the wind turbines by utilizing DSF system still exceeds that of the same quantity of turbines at free-stream at all terrain categories and in all studied cities.

In Melbourne region, by changing the terrain category from TC2 to TC3 and TC4, the AEP of the DSF system reduces 20% and 78% to about 28.6×10^3 *KWh* and 19.3×10^3 *KWh*, respectively. The advantage of utilizing the DSF system in Melbourne is evident by generating 50%, 45% and 43% more energy than wind turbines at a free-stream condition at TC2, TC3 and TC4, respectively. In Sydney region, by changing the terrain category from TC2 to TC3 and TC4, the AEP of the DSF system reduces 23% and 92% to about 16.3 MWh and 10.4 MWh, respectively. However, it is still estimated to generate 29%, 23% and 20% more energy as compared with free-stream wind energy generation at TC2, TC3 and TC4, respectively. In Adelaide region, by changing the terrain category from TC2 to TC3 and TC4, the AEP of the DSF system reduces 24% and 99% to about 13.25 *MWh* and 8.3 MWh, respectively. The wind turbines inside the DSF system as compared with the same quantity in a free-stream condition generate 34%, 28% and 24% more energy in TC2, TC3 and TC4, respectively. In Brisbane region, by changing the terrain category from TC2 to TC3 and TC4, the AEP of the DSF system reduces 26% and 110% to about 10.4 MWh and 6.2 MWh, respectively. The wind turbines inside the DSF system as compared with the same quantity in a free-stream condition generate 28%, 23% and 22% more energy in TC2, TC3 and TC4, respectively.

In general, the increase in the AEP by utilizing the DSF system is less significant in denser built environments. This trend is similar in all cities. This is believed to be associated with the lower amplification factors for lower wind speeds. In other words, by changing the terrain category to

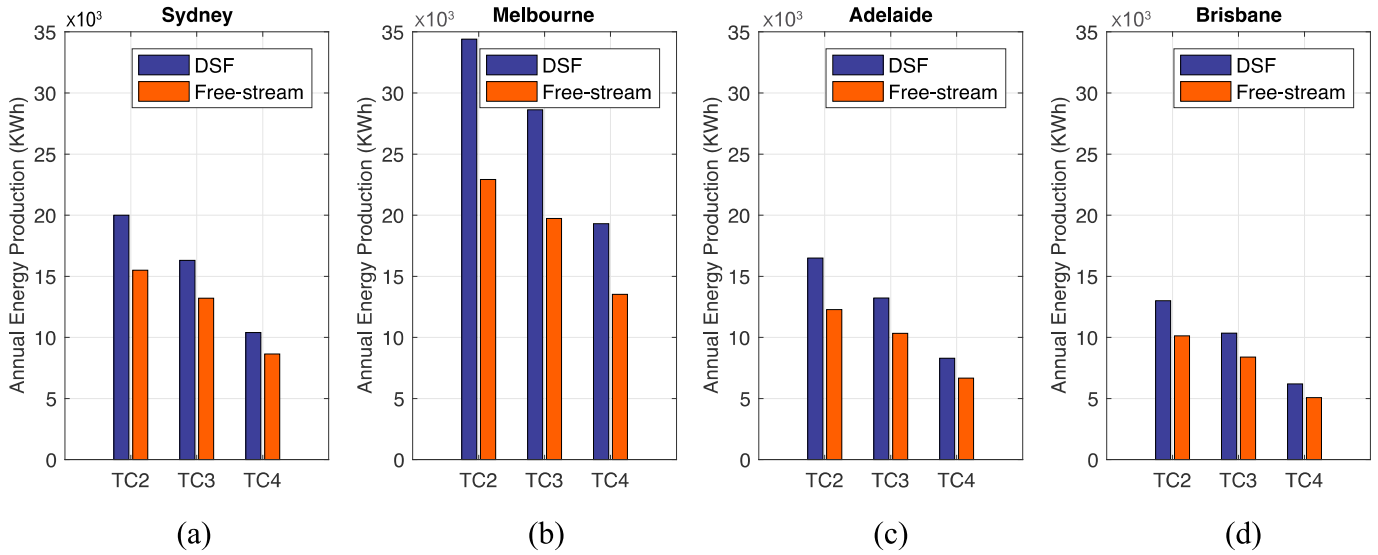

Fig. 11. Annual Energy Production of the HAWTs integrated into the DSF system and in a free-stream condition at different terrain categories in (a) Sydney, (b) Melbourne, (c) Adelaide, and (d) Brisbane

higher levels, the free-stream wind speed decreases which results in an indirect effect of a smaller amplification factor. The two direct (i.e. decrease in the wind speed in denser regions) and indirect (i.e. smaller amplification factor) contributing effects decrease the wind speed inside the corridors and consequently power generation drops.

It was also observed that, the AEP reduction because of changing terrain category to higher levels is less for cities with better AEP performance. For example, while the AEP at TC2 in Melbourne region is 13.4 MWh, this reduces 78% when the terrain changed to TC4. This reduction is 92%, 99% and 110% for Sydney, Adelaide and Brisbane with the AEP of 20, 16.5 and 13 MWh, respectively.

Although this study presents the performance assessment of a special DSF system in the context of four Australian cities and in different terrain surfaces, it could be extended to other urban climates with the metrology provided. The idealistic goal would be to identify the suitable climate characteristics in which the DSF system operates optimal. Moreover, the effect of neighboring buildings in a site-specific assessment and the effect of wind turbines on the flow inside the corridors need to be included in the future studies. The final stage would be a techno-economic assessment of the DSF which involves a comparison study between wind turbines inside the DSF system with stand-alone wind turbines on towers by considering their associated costs and technical aspects.

4. Conclusion

The performance of a special DSF system with strategic openings and aerodynamic modifications for wind energy harvesting purposes was assessed using CFD simulations. A methodology to integrate a local wind data was proposed and four Australian cities of Sydney, Melbourne, Brisbane and Adelaide as cases of study were investigated.

The flow characteristics at the four corridors of the DSF system at different incident wind speeds and directions showed that there is a significant flow enhancement when the wind blows within the range of $\pm 45^{\circ}$ to the corridor axis with the maximum amplification factor of about 1.8 in the leading side corridor. Within this range, the total available wind power was 5.5–6.5 times the power available at $\theta = 0^{\circ}$ when the equal probability of wind in all directions was considered. This indicated a strong bi-directional characteristic of the proposed DSF system. Within this range, the value of total wind power changed marginally, indicating the relative insensitivity of total wind power to the variation in wind directions in this range.

The wind power generation using the DSF system in Sydney and Adelaide was not sensitive to the orientation of the building and DSF system. In contrary, the total wind power in Melbourne and Brisbane showed a strong directional characteristic. The best building orientations to generate power in Melbourne and Brisbane are when the DSF corridor axis is in North-South direction and East-West direction, respectively.

The AEP utilizing an array of 2 by 3 wind turbines, Ampair 300, inside each corridor of a story-high DSF system was determined at the best building orientation of each city. The estimated AEP was 34, 20, 16.5 and 13 MWh in Melbourne, Sydney, Adelaide and Brisbane for TC2. Therefore, Melbourne region with a bi-directional wind characteristic was the most suitable city amongst others in Australia for wind energy harvesting using the proposed DSF system.

In all the cities, changing the terrain category from TC2 to TC3 and to TC4 leads to reduction in the AEP. However, in all studied terrain categories, employing the DSF system results in 20%–50% more AEP than the AEP at the free-stream condition.

In general, it can be concluded that the advantage of utilizing the DSF system depends significantly on local wind characteristics of the region. Moreover, the benefit of utilizing the DSF system over the free-stream wind energy generation in the same region becomes more significant for terrains with smoother roughness.

Acknowledgments

The authors would like to thank MEL Consultants for generously providing directional wind data for four Australian cities used in this study.

Appendix A. Supplementary data

Supplementary data related to this article can be found at https://doi.org/10.1016/j.jweia.2018.02.002.

References

Abohela, I., Hamza, N., Dudek, S., 2013. Effect of roof shape, wind direction, building height and urban configuration on the energy yield and positioning of roof mounted wind turbines. Renew. Energy 50, 1106–1118. https://doi.org/10.1016/j.renene.2012.08.068.

Balduzzi, F., Bianchini, A., Ferrari, L., 2012. Microeolic turbines in the built environment: influence of the installation site on the potential energy yield. Renew. Energy 45, 163–174. https://doi.org/10.1016/j.renene.2012.02.022.

Barbosa, S., Ip, K., 2014. Perspectives of double skin façades for naturally ventilated buildings: a review. Renew. Sustain. Energy Rev. 40, 1019–1029. https://doi.org/10.1016/j.rser.2014.07.192.
Carta, J.A., Ramírez, P., Bueno, C., 2008. A joint probability density function of wind speed and direction for wind energy analysis. Energy Convers. Manag. 49 https://doi.org/10.1016/j.enconman.2008.01.010.
Chaudhry, H.N., Calautit, J.K., Hughes, B.R., 2015. Computational analysis to factor wind into the design of an architectural environment. Model. Simulat. Eng. 2015, 1–10. https://doi.org/10.1155/2015/234601.
Chong, W.T., Wang, X.H., Wong, K.H., Mojumder, J.C., Poh, S.C., Saw, L.H., Lai, S.H., 2016. Performance assessment of a hybrid solar-wind-rain eco-roof system for buildings. Energy Build. 127, 1028–1042. https://doi.org/10.1016/j.enbuild.2016.06.065.
Clean Energy Council, 2016. Clean Energy Australia Report.
Clean Energy Regulator, 2015. Renewable Energy Target, Administrative Report and Annual Statement: Encouraging Investment on Renewable Energy, Clean Energy Regulator. Commonwealth of Australia, Canberra.
Dannecker, R.K.W., Grant, A.D., 2002. Investigations of a building-integrated ducted wind turbine module. Wind Energy 5, 53–71. https://doi.org/10.1002/we.60.
Grant, A., Johnstone, C., Kelly, N., 2008. Urban wind energy conversion: the potential of ducted turbines. Renew. Energy 33, 1157–1163. https://doi.org/10.1016/j.renene.2007.08.005.
Hassanli, S., Hu, G., Fletcher, D.F., Kwok, K.C.S., 2018. Potential application of double skin Façade incorporating aerodynamic modifications for wind energy harvesting. J. Wind Eng. Ind. Aerodyn. 174, 269–280.
Hassanli, S., Hu, G., Kwok, K.C.S., Fletcher, D.F., 2017a. Utilizing cavity flow within double skin façade for wind energy harvesting in buildings. J. Wind Eng. Ind. Aerod. 167, 114–127. https://doi.org/10.1016/j.jweia.2017.04.019.
Hassanli, S., Jafari, S.A., Kwok, K.C.S., 2016. Flow enhancement in tall buildings for wind energy generation. In: 8th International Colloquium on Bluff Body Aerodynamics and Applications. Boston, U.S.
Hassanli, S., Jafari, S.A.H., Eftekharian, E., Kwok, K.C.S., 2017b. Performance assessment of cascaded wind turbines inside through-building openings. In: 9th Asia-Pacific Conference on Wind Engineering. Auckland, New Zealand.
Heath, M.A., Walshe, J.D., Watson, S.J., 2007. Estimating the potential yield of small building-mounted wind turbines. Wind Energy 10, 271–287. https://doi.org/10.1002/we.222.
Heo, Y.G., Choi, N.J., Choi, K.H., Ji, H.S., Kim, K.C., 2016. CFD study on aerodynamic power output of a 110 kW building augmented wind turbine. Energy Build. 129, 162–173. https://doi.org/10.1016/j.enbuild.2016.08.004.
Hu, G., Hassanli, S., Kwok, K.C.S., Tse, K.T., 2017. Wind-induced responses of a tall building with a double-skin façade system. J. Wind Eng. Ind. Aerodyn. 168, 91–100. https://doi.org/https://doi.org/10.1016/j.jweia.2017.05.008.
Jafari, S.A.H., Hassanli, S., Eftekharian, E., Kwok, K.C.S., 2017. Effect of incident wind angle on power generation of building integrated wind turbines. In: 9th Asia-Pacific Conference on Wind Engineering. Auckland, New Zealand.
Khayrullina, A., Van Hooff, T., Blocken, B., 2013. A study on the wind energy potential in passages between parallel buildings. In: 6th European and African Conference on Wind Engineering, EACWE 2013.
Kim, H.-G., Jeon, W.-H., Kim, D.-H., 2016. Wind resource assessment for high-rise BIWT using RS-NWP-CFD. Rem. Sens. 8, 1019.
Kono, T., Kogaki, T., Kiwata, T., 2016. Numerical investigation of wind conditions for roof-mounted wind turbines: effects of wind direction and horizontal aspect ratio of a high-rise cuboid building. Energies 9, 907.
Krishnan, A., Paraschivoiu, M., 2016. 3D analysis of building mounted VAWT with diffuser shaped shroud. Sustain. Cities Soc. 27, 160–166. https://doi.org/10.1016/j.scs.2015.06.006.
Larin, P., Paraschivoiu, M., Aygun, C., 2016. CFD based synergistic analysis of wind turbines for roof mounted integration. J. Wind Eng. Ind. Aerod. 156, 1–13. https://doi.org/10.1016/j.jweia.2016.06.007.
Ledo, L., Kosasih, P.B., Cooper, P., 2011. Roof mounting site analysis for micro-wind turbines. Renew. Energy 36, 1379–1391. https://doi.org/10.1016/j.renene.2010.10.030.
Li, Q.S., Shu, Z.R., Chen, F.B., 2016a. Performance assessment of tall building-integrated wind turbines for power generation. Appl. Energy 165, 777–788. https://doi.org/10.1016/j.apenergy.2015.12.114.
Li, Q.S., Shu, Z.R., Chen, F.B., 2016b. Performance assessment of tall building-integrated wind turbines for power generation. Appl. Energy 165, 777–788. https://doi.org/10.1016/j.apenergy.2015.12.114.
Lu, L., Ip, K.Y., 2009. Investigation on the feasibility and enhancement methods of wind power utilization in high-rise buildings of Hong Kong. Renew. Sustain. Energy Rev. 13, 450–461. https://doi.org/10.1016/j.rser.2007.11.013.
Lu, L., Sun, K., 2014. Wind power evaluation and utilization over a reference high-rise building in urban area. Energy Build. 68, 339–350. https://doi.org/10.1016/j.enbuild.2013.09.029.
Mertens, S., 2003. The energy yield of roof mounted wind turbines. Wind Eng. 27, 507–518. https://doi.org/10.1260/030952403773617472.
Padmanabhan, K.K., 2013. Study on increasing wind power in buildings using TRIZ Tool in urban areas. Energy Build. 61, 344–348. https://doi.org/10.1016/j.enbuild.2012.11.038.
Park, J., Jung, H.J., Lee, S.W., Park, J., 2015. A new building-integrated wind turbine system utilizing the building. Energies 8, 11846–11870. https://doi.org/10.3390/en81011846.
Park, J.H., Chung, M.H., Park, J.C., 2016. Development of a small wind power system with an integrated exhaust air duct in high-rise residential buildings. Energy Build. 122, 202–210. https://doi.org/10.1016/j.enbuild.2016.04.037.
Poirazis, H., 2004. Double Skin Facades for Office Buildings-literature Review Report.
Romanic, D., Rasouli, A., Hangan, H., 2017. Urban wind resource assessment in changing climate: case study. Wind Eng. 41, 3–12. https://doi.org/10.1177/0309524X16653486.
Smith, R.F., Killa, S., 2007. Bahrain World Trade Center (BWTC): the first large-scale integration of wind turbines in a building. Struct. Des. Tall Special Build. 16, 429–439. https://doi.org/10.1002/tal.416.
Tabrizi, A.B., Whale, J., Lyons, T., Urmee, T., 2014. Performance and safety of rooftop wind turbines: use of CFD to gain insight into inflow conditions. Renew. Energy 67, 242–251. https://doi.org/10.1016/j.renene.2013.11.033.
Toja-Silva, F., Colmenar-Santos, A., Castro-Gil, M., 2013. Urban wind energy exploitation systems: behaviour under multidirectional flow conditions - opportunities and challenges. Renew. Sustain. Energy Rev. 24, 364–378. https://doi.org/10.1016/j.rser.2013.03.052.
Toja-Silva, F., Peralta, C., Lopez-Garcia, O., Navarro, J., Cruz, I., 2015a. Roof region dependent wind potential assessment with different RANS turbulence models. J. Wind Eng. Ind. Aerod. 142, 258–271. https://doi.org/10.1016/j.jweia.2015.04.012.
Toja-Silva, F., Peralta, C., Lopez-Garcia, O., Navarro, J., Cruz, I., 2015b. Effect of roof-mounted solar panels on the wind energy exploitation on high-rise buildings. J. Wind Eng. Ind. Aerod. 145, 123–138. https://doi.org/10.1016/j.jweia.2015.06.010.
Walker, S.L., 2011. Building mounted wind turbines and their suitability for the urban scale—a review of methods of estimating urban wind resource. Energy Build. 43, 1852–1862. https://doi.org/10.1016/j.enbuild.2011.03.032.
Wang, B., Cot, L.D., Adolphe, L., Geoffroy, S., Morchain, J., 2015. Estimation of wind energy over roof of two perpendicular buildings. Energy Build. 88, 57–67. https://doi.org/10.1016/j.enbuild.2014.11.072.
Watson, S.J., Infield, D.G., Barton, J.P., Wylie, S.J., 2007. Modelling of the performance of a building-mounted ducted wind turbine. J. Phys. Conf. Ser 75, 12001.
White, L.V., Wakes, S.J., 2014. Permitting best use of wind resource for small wind-turbines in rural New Zealand: a micro-scale CFD examination. Energy Sustain. Dev. 21, 1–6. https://doi.org/10.1016/j.esd.2014.04.003.
Wind roses for selected locations in Australia [WWW Document], n.d. URL http://www.bom.gov.au/climate/averages/wind/selection_map.shtml (accessed 9.28.17).
Yang, A.S., Su, Y.M., Wen, C.Y., Juan, Y.H., Wang, W.S., Cheng, C.H., 2016. Estimation of wind power generation in dense urban area. Appl. Energy 171, 213–230. https://doi.org/10.1016/j.apenergy.2016.03.007.
Zhang, J., Chowdhury, S., Messac, A., Castillo, L., 2013. A multivariate and multimodal wind distribution model. Renew. Energy 51. https://doi.org/10.1016/j.renene.2012.09.026.